RESEARCH ARTICLE | NOVEMBER 03 2025

Structural and optical properties of 100 mm AlN bulk single crystals *⊙*

T. Njuguna 💿 ; H. Alwan 💿 ; K. Hogan; J. Grandusky; J. Li 💿 ; J. Y. Lin 💿 ; H. X. Jiang 🗷 💿



Appl. Phys. Lett. 127, 182102 (2025) https://doi.org/10.1063/5.0300352

A CHORUS





Articles You May Be Interested In

Growth and characterization of high-quality Zr doped AIN epilayers

Appl. Phys. Lett. (January 2025)

Photo-induced electron paramagnetic resonance: A means to identify defects and the defect level throughout the bandgap of ultrawide bandgap semiconductors

Appl. Phys. Lett. (January 2024)

Reliability of NiO/β-Ga₂O₃ bipolar heterojunction

Appl. Phys. Lett. (January 2025)





Structural and optical properties of 100 mm AlN bulk single crystals

Cite as: Appl. Phys. Lett. **127**, 182102 (2025); doi: 10.1063/5.0300352 Submitted: 1 September 2025 · Accepted: 17 October 2025 · Published Online: 3 November 2025







T. Njuguna, 🖟 H. Alwan, 🖟 K. Hogan, J. Grandusky, J. Li, 🖟 J. Y. Lin, 🖟 and H. X. Jiang^{1,a)} 🕞

AFFILIATIONS

¹Department of Electrical and Computer Engineering, Texas Tech University, Lubbock, Texas 79409, USA

ABSTRACT

AlN is a critical ultrawide bandgap (UWBG) semiconductor used in high-power electronics and deep-ultraviolet optoelectronic devices. While 2-in. AlN wafers are commercially available, scaling up to larger diameters is crucial for the widespread adoption of UWBG technology. In this study, we investigated the structural and optical properties of a 100 mm diameter bulk AlN crystal. The transparent regions of the wafer exhibited an x-ray diffraction rocking curve linewidth as low as 27 arcsec and a strong band edge transition at 5.97 eV. However, the wafer showed significant spatial variations in optical transparency. Our detailed characterization results revealed a dominant absorption peak near 2.7 eV, attributed to the presence of aluminum vacancies (V_{Al}); a series of emission peaks involving V_{Al} , V_{Al} — O_N complex, and O_N impurities; and a correlation between less transparent regions and higher concentrations of these specific defects. Understanding the effects of specific impurities/defects on the structural and optical properties is crucial for improving bulk crystal growth and processing methods to produce more uniform, large-diameter AlN substrates, which is vital for the scalable integration of AlN-based devices.

Published under an exclusive license by AIP Publishing. https://doi.org/10.1063/5.0300352

AlN is a critical material for next-generation optoelectronic and high-power electronic devices. $^{1-7}$ Its intrinsic material properties, including a direct ultrawide bandgap (UWBG) of $E_g{\sim}6.1\,{\rm eV},^{1.5}$ high thermal conductivity ($\kappa{\sim}320\,{\rm W/m\,K}),^{8.9}$ large electron mobility ($\mu_e>400\,{\rm cm^2/V\,s}),^{10}$ and exceptionally high critical field ($E_C{\sim}15\,{\rm MV/cm}),^{11}$ combined with its excellent mechanical and chemical stability, render AlN indispensable for applications ranging from deepultraviolet (DUV) emitters and detectors to power-switching devices capable of operating under extreme environments.

AlN and $Al_xGa_{1-x}N$ epilayers grown on foreign substrates such as sapphire and SiC substrates generally possess elevated dislocation densities, primarily due to the pronounced lattice and thermal expansion mismatches between the epilayers and the underlying substrates. The presence of dislocations, defects, and impurities significantly degrades the experimental figure of merit (FOM) of AlN-based devices. Homoepitaxial materials and devices must be utilized to fully exploit the potential of intrinsic properties of AlN, which requires the development of high-quality bulk single-crystal AlN substrates. Beyond their use in homoepitaxy, bulk AlN crystals hold great promise as a host material for a variety of advanced devices, including radiation detectors operating in extreme environments, high-voltage and high-power electronic switches, electro-optic phase modulator and

photonic switches, and field emission devices. Consequently, the development and commercialization of high-quality AlN bulk crystals have progressed rapidly in response to scientific and industrial demand for scalable UWBG semiconductor technologies.

While 2-in. AlN substrates featuring >99% single-crystal coverage and low threading dislocation densities have been commercially available for several years, 12 recent growth advancements have shifted focus toward scaling up substrate diameters while preserving high crystalline quality. Among various approaches, physical vapor transport (PVT) has been established as the dominant technique for bulk AlN crystal growth, owing to its ability to achieve high growth rates and high crystalline quality.¹³ Furthermore, PVT has proven effective in enabling the production of larger diameter wafers, as demonstrated in several recent reports. 13,21,22 This scalability is attributed to the progressive lateral enlargement of the seed crystal and innovations in crucible design and thermal field optimization within the PVT growth system, allowing for diameter scaling with minimal degradation in crystalline quality. Notably, Bondokov et al. reported a fourfold increase in wafer area with only a 10%-20% increase in resource consumption, while maintaining comparable crystallinity and growth rate. 13 The 100 mm AlN single-crystal substrates were first introduced in 2023, exhibiting 80%–90% of usable area, representing a significant

²Crystal IS Inc., Green Island, New York 12183, USA

a) Author to whom correspondence should be addressed: hx.jiang@ttu.edu

step toward commercial deployment. ¹³ Subsequent developments have demonstrated further improvements, with recent high-purity PVT-grown AlN boules achieving >99% usable area following slicing and polishing for epitaxy ready applications. ¹³

For 100 mm AlN substrates, unintentional incorporation of common impurities such as carbon (*C*), oxygen (O), and silicon (Si) has been reported. ¹³ Furthermore, as illustrated in Fig. 1, the presence of defects/impurities also gives rise to visible wavelength color centers, leading to spatial variations in optical transparency across the wafer surface. ¹³ These optical signatures provide a qualitative indication of impurity incorporation and defect inhomogeneity across the substrate. While considerable progress has been made in characterizing and identifying the physical origins of unintentional impurities and defects in AlN, further investigation is required to fully classify these centers and to understand the effect on device relevant properties.

Here, we report results of the structural and optical characterization conducted on a 100 mm diameter bulk AlN wafer of thickness $600 \, \mu \text{m}$ produced by Crystal IS using the PVT technique. The growth conditions were described in detail in a previous publication by Bondokov et al. 13 Briefly, the AlN source was placed in a tungsten crucible which also contained 3-in. AlN seeds. The crucible was heated to a temperature well above 2000 °C using radio frequency (RF) heating.¹³ Various characterization techniques, including x-ray diffraction (XRD), x-ray photoelectron spectroscopy (XPS), optical absorption, and photoluminescence (PL) emission spectroscopy were employed, with the aim to provide insights into the physical origins of defect/ impurity centers that contributed to spatial variations in optical transparency across the wafer surface. As shown in Fig. 1, optical transparency variations across the wafer surface are highly visible. We focus on two representative areas labeled (a) and (b), where area (a) appears more transparent and area (b) appears darkish. Our analysis focused

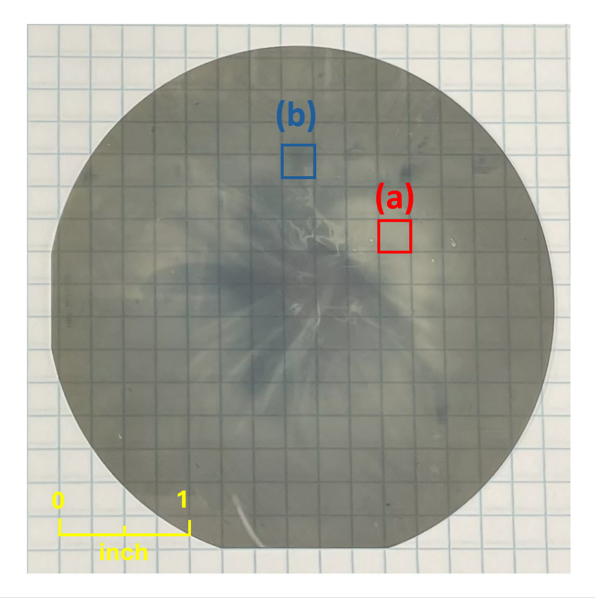


FIG. 1. Optical image of a 100 mm diameter c-plane bulk AlN wafer with a thickness of $600 \, \mu \text{m}$ (Al-surface) grown via physical vapor transport (PVT) method. Two regions exhibiting distinct optical transparency are highlighted: (a) a region with higher transparency, and (b) a darkish region with lower transparency.

on the Al-terminated surface, which was processed and polished for epi-ready application.

Figure 2 compares XRD characterization results between the two selected regions of the AlN substrate: area (a) and area (b). Both ω –2 θ scans and ω -scans (rocking curves) were performed. Compared to the XRD results of area (b), the more transparent region (Area a) exhibits a slightly higher AlN (002) diffraction peak intensity and narrower full width at half maximum (FWHM) in the ω –2 θ scan. Moreover, the rocking curves of the (002) peaks shown in Fig. 2(b) reveal a significantly narrower FWHM in the transparent region (Area a) than the darkish region (Area b), 27 vs 70 arc sec. The results indicate that darkish color is likely influenced by the presence of higher concentrations of defect and impurity related scattering centers that locally degrade optical and structural quality.

To assess the correlation between the presence of unintentional carbon (C) and oxygen (O) impurities and optical and structural quality, we carried out XPS studies for the two regions. The measurements were performed on a Physical Electronics PHI 5000 Versa Probe II Hybrid system under high vacuum conditions ($\sim 10^{-7}$ Torr). Because XPS is a surface-sensitive technique, successive argon (Ar) ion sputtering was used to remove the top layers until the measured concentrations of C and O impurities remained constant. This process removed surface contaminants by carbon and oxygen, which are commonly present from atmospheric exposure, allowing for a more reliable comparison of the true subsurface composition of the samples.

Our analysis focused on comparing the relative carbon and oxygen impurities, as well as the relative Al and N contents in area (a) and area (b). Figure 3 presents the XPS spectra obtained from regions (a) and (b), indicating the binding energy positions and corresponding atomic concentrations for the elements under investigation. In both regions, N concentrations exceeded those of Al. Area (a) and area (b) exhibited 51% and 46.1% N concentration, respectively, while their respective Al concentration was 48.8% and 44.6%. The results indicate that the AlN wafer studied here is Al-deficient, suggesting the presence of V_{Al} in AlN wafers. Moreover, the concentrations of Al and N are lower in area (b) than those in area (a) due to higher O and C impurity concentrations, which were measured to be at 4.6% and 4.7% atomic concentrations, respectively. While XPS may drastically overestimate the absolute concentrations of C and O impurities, the results clearly show that the darker areas (b) contain higher concentrations of C and O than the more transparent regions.

In fact, the C and O concentrations in the more transparent region (a) are quite low, with O < 0.1% and C < 0.2%, which can be considered negligibly low because of the limited instrument resolution. Impurity concentrations have been directly measured for similar 100 mm AlN wafers by Bondokov et al. using secondary ion mass spectrometry (SIMS).¹³ On average, the concentrations of C and O are below 10¹⁷ cm⁻³ and the concentration of Si was almost at the detection limit of the instrument $(5 \times 10^{16} \text{ cm}^{-3})$. Thus, we expect the impurity concentrations in the more transparent area (a) to be below 10¹⁷ cm⁻³ as previously reported by Bondokov et al. On the other hand, for the less transparent area (b), the measured \sim 4% impurity concentration by XPS indicates that the O and C impurity concentrations are above $10^{17} \, \text{cm}^{-3}$. The components of the growth chamber and subsequent wafer processing stages were considered the source of these impurities. 13 Continuing efforts on controlling process and cleanliness to AlN source preparation are also needed. The combination of

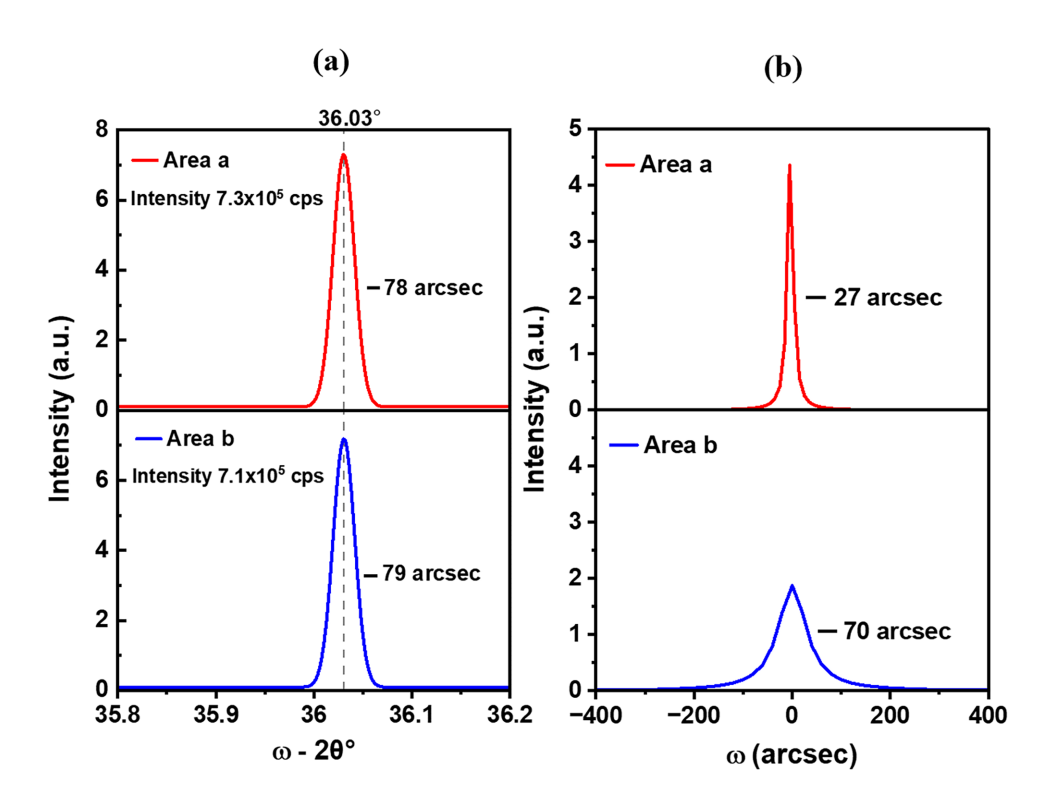


FIG. 2. (a) XRD ω – 2θ scans and (b) XRD ω -scans or rocking curves of the (002) planes of AIN substrate measured at different areas of area (a) and area (b) as designated in Fig. 1.

Al deficiency and higher impurity concentrations in the less transparent area (b) suggests the likely presence of V_{Al} . Moreover, when oxygen impurities substitute on the nitrogen sites (O_N) , they act as donors, and the incorporation of O_N , during growth can cause Fermi level shifting toward the conduction band edge, significantly reducing the formation energies, and enhancing the formation of V_{Al} and Al vacancy and O impurity complexes $(V_{Al}-O_N)^{24}$

To probe sub-bandgap absorption due to the presence of defects, optical absorption measurements were carried out from 1.5 to 5 eV using an Agilent Cary 5000 UV-vis-NIR spectrophotometer and the results are shown in Fig. 4. The resultant spectra in Fig. 4 showed that the darkish area (b) has a higher absorbance all the way into the deep UV region, implying dislocations, defects, and impurities are more numerous in area (b) than in area (a), which corroborates with the XRD and XPS results shown in Figs. 2 and 3. However, the measured absorption coefficients in this spectral region are about 4 orders of magnitude smaller than that of the fundamental band edge absorption in AlN of \sim 2 \times 10⁵ cm^{-1,1} which is a typical signature of optical absorption due to dislocations, defects, and impurities. Moreover, the measured sub-band absorption coefficients in the spectral range of 4–5 eV are at least one order of magnitude lower than those of previous reported values for AlN bulk crystals produced by the PVT method²⁵ and similar to the recent reported values for 2 in. AlN bulk wafers produced by PVT, 26 indicating that the overall optical quality of this 100 mm AlN wafer has been significantly improved and is on par with those of 2 in. wafers.

Notably, both areas (a) and (b) exhibit a distinct absorption peak at 2.75 eV. Slack *et al.* reported an absorption peak at 2.86 eV, attributing to nitrogen vacancies (V_N) . Bickermann *et al.* reported an absorption peak at \sim 2.8 eV in PVT-grown polycrystalline bulk AlN

and observed a direct correlation between the absorption peak intensity and the growth temperature, which supported the interpretation of the absorption peak originating from an intrinsic defect with a temperature-dependent formation probability. Other proposed mechanisms include a transition involving V_{Al} and N vacancy $(V_{\rm N})$ and oxygen impurities, a donor–acceptor pair transition between the $V_{\rm N}$ and substitutional carbon $(C_{\rm N})$ impurities, and a band-to-impurity transition involving isolated V_{Al} .

It is important to note that the strengths of the absorption peak at 2.75 eV in both area (a) and area (b) are comparable, even though the O and C impurity concentrations in areas (a) and (b) are vastly different. Moreover, XPS results confirmed that both area (a) and area (b) of the sample are Al deficient. Therefore, we believe that the absorption peak at 2.75 eV is most likely linked to V_{Al} , involving isolated V_{Al} or $V_{Al}-O_N$ complex.

Further analysis of the two regions was performed using PL emission spectroscopy. The PL system consists of an Excimer laser $(\lambda_{\rm exc}=193\,{\rm nm},\,6.42\,{\rm eV})$ as an excitation source, and a fiber-coupled optical spectrometer for dispersing the emission signal. As shown in Fig. 5(a), both regions exhibit a strong band edge emission centered at 5.97 eV. The darker area (b) exhibits a slightly higher band edge intensity than the more transparent region of area (a), in contrast to the expectation, hypothesizing a higher band edge emission intensity in the more transparent region with higher crystalline quality. PL spectra were also taken across the entire wafer in the middle vertical line to include a few transition regions, as illustrated in the inset of Fig. 5(b). Figure 5(b) plots the overall PL "mapping" results, which revealed that the overall PL spectral features are very similar with some variations in the emission intensity of the 5.97 eV line. Defect transitions were noted in all regions probed. The PL spectrum of more transparent area

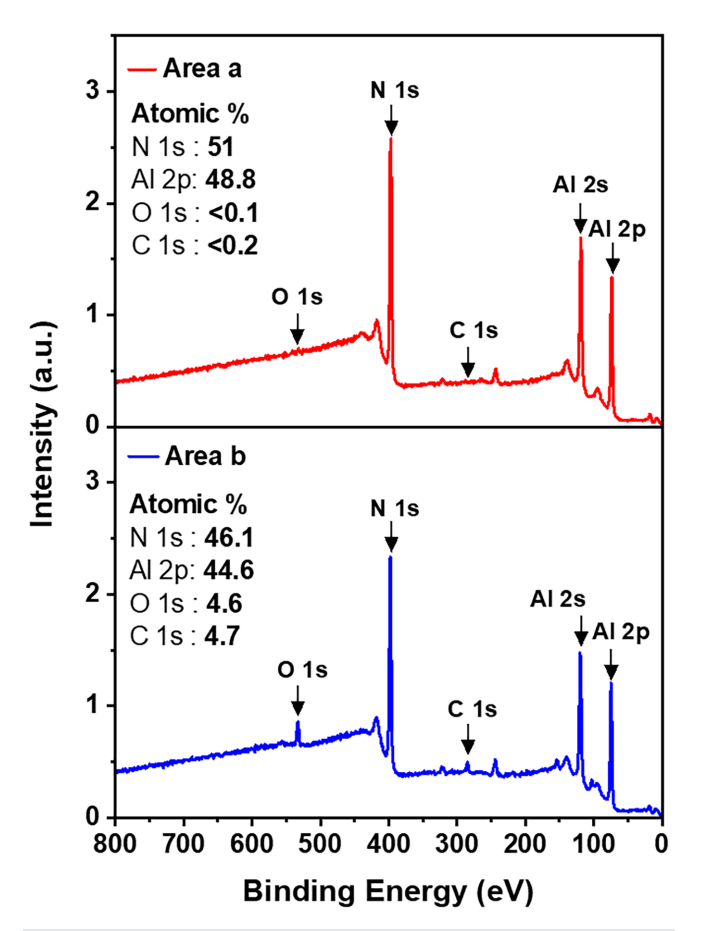


FIG. 3. XPS survey spectra performed on an AIN at area (a) and area (b). Relative atomic concentrations for N 1s, Al 2p, O 1s, and C 1s are indicated in the figure.

(a) resolved two prominent peaks near 2.2 and $3.9\,\mathrm{eV}$. The $3.9\,\mathrm{eV}$ emission line has been observed in AlN bulk crystals grown by the PVT method and linked to the presence of C_N^- point defect. In contrast, the spectra in all other locations, including area (b), show a very broad band covering the range from 2 to $5\,\mathrm{eV}$, which signifies the inclusion of multiple impurity/defect-related transition bands, corroborating with XRD, XPS, and optical absorption results and revealing a locally degraded structural and optical quality of darkish regions.

It is difficult to examine the defect transitions in more detail under the above bandgap excitation because the band edge transition at 5.97 eV is overwhelmingly dominant. To further analyze impurity/ defect transitions, a below-bandgap excitation was employed to minimize the band edge recombination processes using a frequency tripled Ti:sapphire laser with an excitation wavelength of 260 nm. A 1.3 m monochromator coupled with a microchannel plate photomultiplier tube (MCP-PMT) was used to disperse the PL signal and the resulting 300 and 10 K PL spectra are shown in the top and bottom panels of Fig. 6, respectively. Notably, a peak at 2.15 eV is observable in both areas (a) and (b) and is very close to an emission line occurring at 2.1 eV observed in AlN epilayers, which has been ascribed to a band-to-impurity transition involving $V_{Al} - O_N$ complexes in the basal configuration. 30 A broad emission peak centered at approximately 3.73 eV

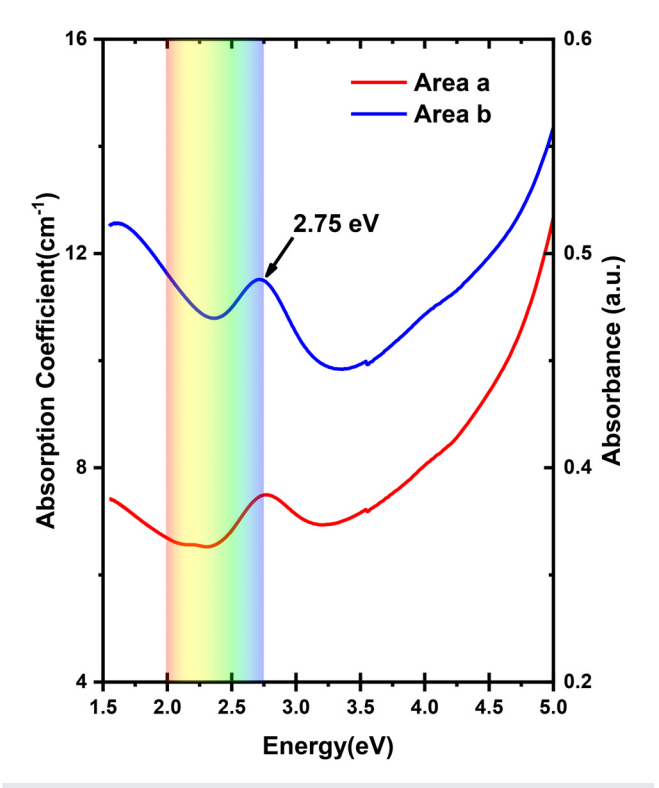


FIG. 4. Sub-bandgap optical absorption spectra for area (a) and area (b). The color gradient shows the transition of visible light from red to violet.

is also observed in both area (a) and area (b). Moreover, the room temperature PL spectrum of the more transparent area (a) exhibits a sharper peak at 2.64 eV, whereas the less transparent area (b) exhibits multiple broad peaks in between 2.15 and 3.75 eV.

Overall, the intensities of the observed emission peaks in both areas (a) and (b) are comparable, despite significant differences in the O and C impurity concentrations. This suggests that these emission lines are not directly tied to these bulk impurities. However, the emission peak positions align closely with those obtained by a hybrid functional calculation, which predicted four band-to-impurity emission lines involving deep acceptor states of isolated V_{Al} and $V_{Al}-O_N$ complexes in AlN. Given that the 100 mm wafer studied here is Al-deficient, we believe that the observed emission lines are related to V_{Al} and $V_{Al}-O_N$ complexes.

The low temperature (10 K) PL spectra shown in the bottom panels of Fig. 6 further strengthened our interpretation. Compared to 300 K spectra shown in the top panels, the overall emission intensities of defect transitions in both area (a) and area (b) increased by four times at 10 K. More significantly, in both area (a) and area (b), the broad peak appearing around 2.7–2.8 eV becomes overwhelmingly dominant, which matches almost perfectly with those predicted for the band-to-impurity transitions involving isolated V_{Al} . More specifically, the previous hybrid functional calculation predicted that the transition between the conduction band and the V_{Al} deep acceptor, described by the process of $e + V_{Al}^{2-} \rightarrow h\nu$ (2.73 eV) + V_{Al}^{3-} gives rise to a 2.73 eV photon, whereas the transition between the V_{Al} deep acceptor and valence band, described by the process of $V_{Al}^{3-} + h \rightarrow h\nu$ (2.77 eV) + V_{Al}^{2-} gives

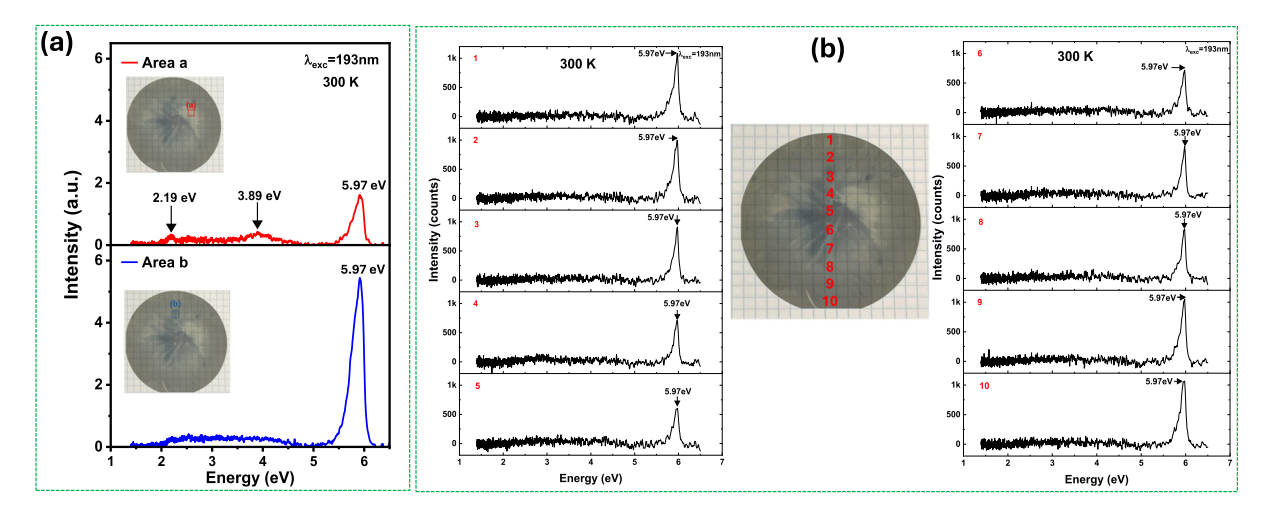


FIG. 5. Room temperature (T = 300 K) PL spectra of AIN excited by an Excimer laser (λ_{exc} = 193 nm) with an average power of 4 W: (a) measured at (a) area (b); (b) measured at 10 different locations along the middle vertical line across the wafer as indicated in the inset.

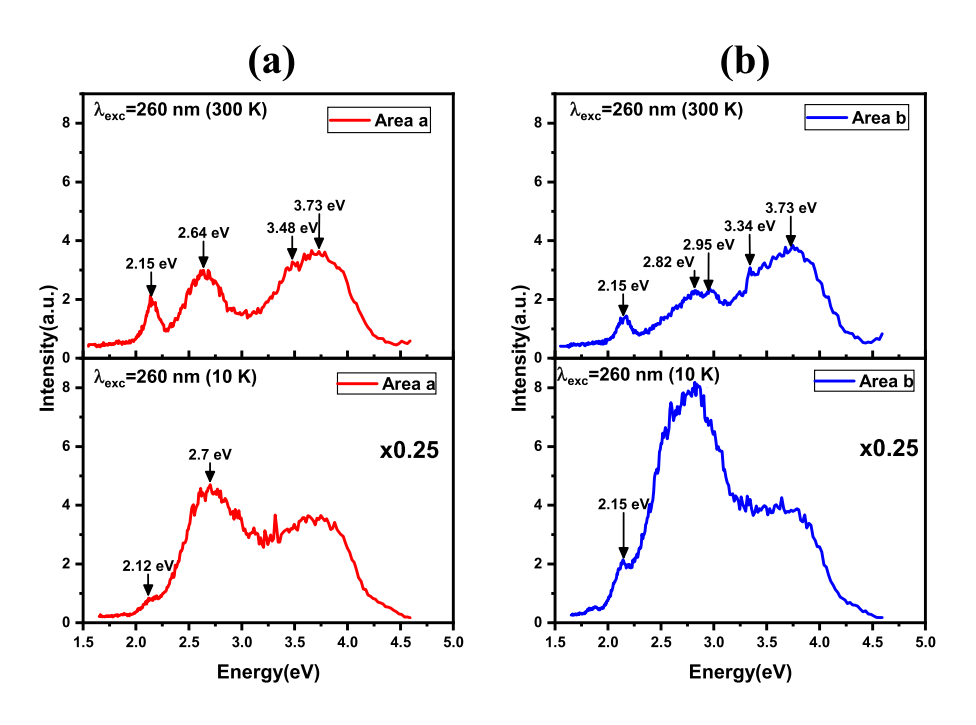


FIG. 6. Room temperature (top panels) and 10 K (bottom panels) PL spectra of AlN excited by a frequency tripled Ti:sapphire laser ($\lambda_{\rm exc} = 260$ nm), measured at (a) area (a) and (b) area (b).

rise to a 2.77 eV photon. The broad peak in the high energy side in the 3.3–3.8 eV spectral region observed in both area (a) and area (b) is also reasonably close to those predicted (3.24 and 3.46 eV) for the band-to-impurity transitions involving $(V_{Al} - O_N)$ and $(V_{Al} - 2O_N)$ deep acceptors. The precise peak positions can vary in different samples and different sample locations in the case here, as varying impurity concentrations can lead to the formation of different defect complex types (e.g., $V_{Al} - O_N$ vs $V_{Al} - 2O_N$), charge states, and bonding configurations arising from Al–N bond anisotropy. It is worth noting that the emission line near 3.9 eV, previously linked to C impurities, was not clearly resolved in the PL spectra shown in Fig. 6. However, it was

distinguishable in the PL spectrum in Fig. 5 for area (a), where C and O impurity contents are low.

In summary, we have investigated the non-uniform optical transparency of a recently available 100 mm AlN bulk crystal. The results provide considerable insights into further improving the purity of bulk AlN substrates for commercial use. The results showed that the darkish and less transparent areas are directly linked to higher concentrations of unintentional impurities and defects. Photoluminescence emission and optical absorption spectroscopy results showed strong impurity related transitions in the range of $2-4\,\mathrm{eV}$ linked to the presence of $V_{Al},\,V_{Al}-O_N$, and C_N . These findings indicate that the

incorporation of C and O impurities and hence the generation of V_{Al} -related defects is nonuniform across the wafer, which also causes structural and optical transparency nonuniformity across the wafer. To improve the quality and purity of AlN wafers, introducing strategies for reducing carbon and oxygen contamination from source materials and growth process environment is highly desirable. While a high growth rate is desired for production, decreasing the growth rate may aid in suppressing the formation of V_{Al} and V_{Al} -complexes. Hence, finding a balance between an acceptable growth rate and low impurity concentrations is an important area for future study. Moreover, since defect formation exhibits an exponential dependence on the growth temperature, there is still room for growth temperature optimization to minimize the incorporation impurities/defects while maintaining acceptable crystalline quality. Monitoring structural and optical properties for materials produced under different conditions can guide the growth process toward achieving high purity, large diameter AlN bulk substrates needed for the next generation of UWBG semiconductor devices.

The information, data, or work presented herein was funded in part by the Advanced Research Projects Agency-Energy (ARPA-E), U.S. Department of Energy, under ULTRAFAST program, Award No. DE-AR0001821, monitored by Dr. Johan Enslin, Dr. Olga Spahn, and Dr. Eric Carlson. The views and opinions of authors expressed herein do not necessarily state or reflect those of the United States Government or any agency thereof. Jiang and Lin are grateful to the AT&T Foundation for the support of Ed Whitacre and Linda Whitacre endowed chairs.

AUTHOR DECLARATIONS Conflict of Interest

The authors have no conflicts to disclose.

Author Contributions

T. Njuguna: Data curation (equal); Formal analysis (equal); Investigation (equal); Methodology (equal); Software (equal); Validation (equal); Visualization (equal); Writing - original draft (equal). H. Alwan: Data curation (equal); Formal analysis (equal); Investigation (equal); Methodology (equal); Software (equal); Validation (equal); Visualization (equal); Writing - original draft (equal). K. Hogan: Investigation (equal); Methodology (equal); Validation (equal); Visualization (equal). J. Grandusky: Investigation (equal); Methodology (equal); Validation (equal); Visualization (equal). J. Li: Data curation (equal); Formal analysis (equal); Investigation (equal); Methodology (equal); Project administration (equal); Resources (equal); Software (equal); Supervision (equal); Validation (equal); Visualization (equal). J. Y. Lin: Conceptualization (equal); Formal analysis (equal); Funding acquisition (equal); Investigation (equal); Methodology (equal); Project administration (equal); Resources (equal); Supervision (equal); Validation (equal); Visualization (equal); Writing - review & editing (equal). H. X. Jiang: Conceptualization (equal); Formal analysis (equal); Funding acquisition (equal); Investigation (equal); Methodology (equal); Project administration (equal); Resources (equal); Supervision (equal); Validation (equal); Visualization (equal); Writing - review & editing (equal).

DATA AVAILABILITY

The data that support the findings of this study are available within the article.

REFERENCES

- ¹P. B. Perry and R. F. Rutz, "The optical absorption edge of single-crystal AlN
- prepared by a close-spaced vapor process," Appl. Phys. Lett. 33, 319 (1978). ²Z. Cheng, Y. R. Koh, A. Mamun, J. Shi, T. Bai, K. Huynh, L. Yates, Z. Liu, and R. Li, "Experimental observation of high intrinsic thermal conductivity of AlN," Phys. Rev. Mater. 4, 044602 (2020).
- ³S. Nakamura, T. Mukai, and M. Senoh, "Candela-class high-brightness InGaN/ AlGaN double-heterostructure blue-light-emitting diodes," Appl. Phys. Lett. 64, 1687 (1994).
- ⁴W. A. Doolittle, C. M. Matthews, H. Ahmad, K. Motoki, S. Lee, A. Ghosh, E. N. Marshall, A. L. Tang, P. Manocha, and P. D. Yoder, "Prospectives for AlN electronics and optoelectronics and the important role of alternative synthesis," Appl. Phys. Lett. 123, 070501 (2023).
- J. Li, K. B. Nam, M. L. Nakarmi, J. Y. Lin, H. X. Jiang, P. Carrier, and S.-H. Wei, "Band structure and fundamental optical transitions in wurtzite AlN," Appl. Phys. Lett. 83, 5163 (2003).
- ⁶Y. Taniyasu, M. Kasu, and T. Makimoto, "An aluminium nitride light-emitting diode with a wavelength of 210 nanometres," Nature 441, 325 (2006).
- ⁷Z. Zhang, M. Kushimoto, T. Sakai, N. Sugiyama, L. J. Schowalter, C. Sasaoka, and H. Amano, "A 271.8 nm deep-ultraviolet laser diode for room temperature operation," Appl. Phys. Express 12, 124003 (2019).
- ⁸G. A. Slack, "Nonmetallic crystals with high thermal conductivity," J. Phys. Chem. Solids 34, 321 (1973).
- ⁹R. L. Xu, M. M. Rojo, S. M. Islam, A. Sood, B. Vareskic, A. Katre, N. Mingo, K. E. Goodson, H. G. Xing, D. Jena, and E. Pop, "Thermal conductivity of crystalline AlN and the influence of atomic-scale defects," J. Appl. Phys. 126, 185105 (2019).
- 10 Y. Taniyasu, M. Kasu, and T. Makimoto, "Increased electron mobility in n-type Si-doped AlN by reducing dislocation density," Appl. Phys. Lett. 89, 182112
- ¹¹T. L. Chu and R. W. Kelm, "The preparation and properties of aluminum nitride films," J. Electrochem. Soc. 122, 995 (1975).
- ¹²R. T. Bondokov, J. Mark, K. Hogan, G. Norbury, and J. Grandusky, "Growth of bulk AlN crystals," in Comprehensive Semiconductor Science and Technology, 2nd ed., edited by R. Fornari (Elsevier, 2025), pp. 132-158.
- ¹³R. T. Bondokov, K. Hogan, G. Q. Norbury, S. Matsumoto, and J. Grandusky, "Development of 100 mm AlN single-crystal growth and subsequent substrate preparation," Phys. Status Solidi B 2500032 (2025).
- 14. Alwan, N. K. Hossain, J. Li, J. Y. Lin, and H. X. Jiang, "Growth and characterization of high-quality Zr-doped AlN epilayers," Appl. Phys. Lett. 126, 022106 (2025).
- 15 R. Gaska, C. Chen, J. Yang, E. Kuokstis, A. Khan, G. Tamulaitis, I. Yilmaz, M. Shur, J. Rojo, and L. Schowalter, "Deep-ultraviolet emission of AlGaN/AIN quantum wells on bulk AIN," Appl. Phys. Lett. 81, 4658 (2002).
- ¹⁶J. Li, Z. Y. Fan, R. Dahal, M. L. Nakarmi, J. Y. Lin, and H. X. Jiang, "200 nm deep ultraviolet photodetectors based on AlN," Appl. Phys. Lett. 89, 213510 (2006).
- ¹⁷Y. H. Chen, J. Encomendero, C. Savant, V. Protasenko, H. G. Xing, and D. Jena, "Electron mobility enhancement by electric field engineering of AlN/GaN/AlN quantum-well HEMTs on single-crystal AlN substrates," Appl. Phys. Lett. 124(15), 152111 (2024).
- ¹⁸R. T. Bondokov, S. G. Mueller, K. E. Morgan, G. A. Slack, S. Schujman, M. C. Wood, J. A. Smart, and L. J. Schowalter, "Large-area AlN substrates for electronic applications: An industrial perspective," J. Cryst. Growth 310, 4020
- ¹⁹R. R. Sumathi, "Review Status and challenges in hetero-epitaxial growth approach for large diameter AlN single crystalline substrates," ECS J. Solid State Sci. Technol. 10, 035001 (2021).
- ²⁰R. T. Bondokov, K. Hogan, G. Q. Norbury, J. Mark, S. P. Branagan, N. Ishigami, J. Grandusky, and J. Chen, "Development of 3-inch AlN Single Crystal Substrates," ECS Trans. 109, 13 (2022).

- ²¹C. Hartmann, M. P. Kabukcuoglu, C. Richter, A. Klump, D. Schulz, U. Juda, M. Bickermann, D. Hanschke, R. Schroder, and T. Straubinger, "Efficient diameter enlargement of bulk AlN single crystals with high structural quality," Appl. Phys. Express. 16, 075502 (2023).
- ²²R. T. Bondokov, S. P. Branagan, J. Grandusky, K. Hogan, J. Mark, and J. Chen, "Control of basal plane dislocations in large aluminum nitride crystals," U.S.
- patent US12163250B1 (12 October 2024).

 23T. Erlbacher, M. Bickermann, B. Kallinger, E. Meissner, A. J. Bauer, and L. Frey, "Ohmic and rectifying contacts on bulk AlN for radiation detector applications," Phys. Status Solidi C 9, 968 (2012).
- ²⁴Q. Yan, A. Janotti, M. Scheffler, and C. G. Van de Walle, "Origins of optical absorption and emission lines in AlN," Appl. Phys. Lett. 105, 111104 (2014).
- ²⁵G. A. Slack, L. J. Schowalter, D. Morelli, and J. A. Freitas, Jr., "Some effects of oxygen impurities on AlN and GaN," J. Cryst. Growth 246, 287 (2002).
- ²⁶S. I. Mollik and M. E. Zvanut, "Ultraviolet absorption of point defects in high purity bulk AlN," AIP Adv. 15, 045203 (2025).

 27M. Bickermann, B. M. Epelbaum, and A. Winnacker, "Characterization of bulk
- AlN with low oxygen content," J. Cryst. Growth 269, 432 (2004).
- ²⁸D. Alden, J. S. Harris, Z. Bryan, J. N. Baker, P. Reddy, S. Mita, G. Callsen, A. Hoffmann, D. L. Irving, R. Collazo, and Z. Sitar, "Point-defect nature of the ultraviolet absorption band in AlN," Phys. Rev. Appl. 9, 054036
- ²⁹A. Sedhain, L. Du, J. H. Edgar, J. Y. Lin, and H. X. Jiang, "The origin of 2.78 eV emission and yellow coloration in bulk AlN substrates," Appl. Phys. Lett. 95, 262104 (2009).
- 30 A. Sedhain, J. Y. Lin, and H. X. Jiang, "Nature of optical transitions involving cation vacancies and complexes in AlN and AlGaN," Appl. Phys. Lett. 100, 221107 (2012).